Portable Microwave (pMWI) System for Brain Stroke Imaging Using Off-the-Shelf Components

Portable Microwave (pMWI) System for Brain Stroke Imaging Using Off-the-Shelf Components

M. Gugliermino†, D. O. Rodriguez-Duarte†, C. Origlia†, J. A. Tobon Vasquez†
R. Scapaticci*, L. Crocco*, F. Vipiana†
†Dept. Electronics and Telecommunications, Politecnico di Torino, Turin, Italy
*Institute for Electromagnetic Sensing of the Environment, National Research Council, CNR, Naples, Italy
francesca.vipiana@polito.it

***Abstract* — This paper presents an upgraded version of a low-complexity microwave imaging (MWI) system for brain stroke monitoring using an off-the-shelf solid-state switching matrix, named correlator, and new optimized antenna-matching cells (Ant-MM). The new system architecture comprises a four-port transceiver made of two compact Vector Network Analyzers (VNA) in parallel, two 4-by-16 correlators, and twenty-two Ant-MMs placed on a head phantom as a helmet. The imaging consists of a qualitative linear inversion algorithm with low computing demand, running on a conventional laptop and retrieving 3-D dielectric contrast maps in real-time. As validation, the system is experimentally tested in a simplified but realistic mimicked hemorrhagic scenario using anthropomorphic phantoms, demonstrating its capability to image the stroke affection. Overall, the upgraded scanner keeps its imaging performance while reducing size at a portable or bedside patient level and data acquisition time.**

***Keywords* — Biomedical microwave imaging, brain stroke monitoring, inverse scattering, solid-state switching matrix.**

I. Introduction

A cerebrovascular incident, commonly known as a stroke, is a critical medical condition that precipitates the decay of brain tissue due to an inadequate supply of oxygen and nutrients. This deficiency typically arises from a tumultuous disruption in blood flow within the brain, whether triggered by a ruptured brain artery, a leak in the blood vessels, or a blood clot. It echoes across the global healthcare landscape, standing as a problematic challenge with far-reaching implications for individual well-being and, in critical instances, posing life-threatening consequences [1]. So, minimizing brain damage and optimizing recovery prospects accentuate the pivotal role of prompt medical intervention and post-onset monitoring, which currently relies on image-based diagnostic gold standards, such as magnetic resonance (MRI) and computed tomography (CT) [2].

However, these alternatives have intrinsic drawbacks regarding portability, safeness (in the CT case due to the use of ionizing radiation), availability, data acquisition time, and investment and maintenance costs, that limit their use in stroke management protocols in pre-hospital and post-event follow-up scenarios, and restricting it to the initial medical assessment in most of the cases, when are available [3]. This situation has beckoned the exploration of alternative technological avenues of medical support [4]–[6], including portable CT/MRI (pCT/pMRI) [7]–[9], near-infrared spectroscopy (NIRS), ultrasound (US), electroencephalography (EEG), volumetric impedance phase-shift spectroscopy (VIPS), and microwave technology (MWI) [10]–[14].

In specific, MWI is a technology that is non-ionizing, low-intensity, and cost-effective approach enabling pre-hospital diagnosis, bedside brain imaging, and continuous monitoring during the post-acute stage. The aftermath of a stroke induces distinctive changes in the physiological characteristics of affected brain tissues, manifesting as alterations in their dielectric properties. In the case of a hemorrhage (HS), the tissue's permittivity increases due to bleeding, while in ischemia (IS), it decreases owing to reduced oxygen supply [15]. Then, by analyzing the back-scattered response of a region of interest exposed to an electromagnetic (EM) field at microwave frequencies, MWI unveils a spatial distribution of the electric contrast within the examined area through specialized inversion algorithms.

This work introduces an upgraded version of the low-complexity MWI scanner reported in [16], [17]. Notably, this third iteration propose a new architecture that substitutes traditional electromechanical switches with state-of-the-art off-the-shelf solid-state alternatives [18]. This transformation not only accelerates switching times but also enhances the system's portability and stability, ultimately extending its durability and lifespan. Moreover, the system employs a new simplified and optimized antenna-matching sensor. Hence, the new proposed system is validated performing imaging of a mimicked hemorrhagic scenario, demonstrating this keeps the capabilities to detect and follow-up an evolving stroke condition in real-time.

In the following, Sect. II delineates the upgraded hardware implementation, focusing on the renewed switching component. Then, Sect. III covers the validation on a simplified head phantom mimicking a hemorrhagic situation, closing with the conclusions and future perspectives in Sect. IV.

II. Upgraded Portable MWI System

The upgraded portable MWI (pMWI) system depicted in Fig. 1 is essentially characterized by three main components that record sequentially multi-view scattering measures: (1) a four-port transceiver, (2) a four-by-twenty-two multiplexing interface, and (3) twenty-two radiating units. Then, a standard laptop sets and controls the system and runs a differential

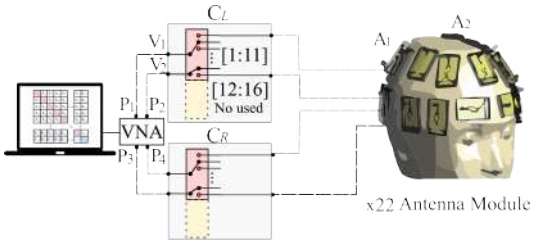

(a)

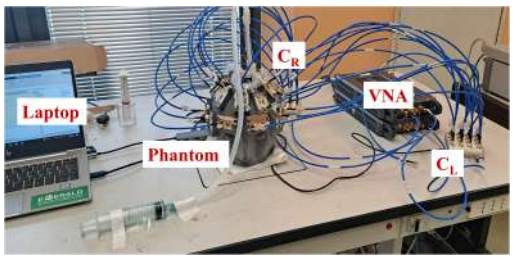

(b)

Fig. 1. Upgraded pMWI system: (a) 4×24 architecture scheme and (b) experimental setup.

linear imaging inversion algorithm based on distorted Born approximation and a truncated singular value decomposition (TSVD) with removal artifact features as described in [17]. Moreover, the input measured scattering matrix are de-embedded compensating the different electrical lengths in the correlators[19]. The latter employs an imaging kernel build using a full-wave digital twin simulated with in-house Finite Element Method (FEM) solver [20].

A. *Transceiving System*

The microwave scanner comprises a four-port transceiver system utilizing two compact Keysight Streamline USB Vector Network Analyzer (VNA), specifically the P9375A model, configured in parallel [21]. It serves the dual purpose of providing the stimulus and capturing the response, and is set as follows: a frequency band ranging from 0.8 to 1.8 GHz, 11 sweep points, power to 0 dBm, and intermediate frequency filter (IF) to 100 Hz. This configuration maintain adequate signal integrity for the application.

B. *Multiplexing Interface*

This stage enables multiplexing of the four ports of the transceiving with the twenty-two Ant-MM cells (radiating units), avoiding the complexity and cost of using 22-ports VNA. Specifically, in this system version, we employ the correlator EVT1016 [18]. This is an off-the-shelf solid-state switching matrix, and it allows us to replace the ad-hoc electromechanical one previously used in [16], [17] or the need for a custom-made solid-state one as in [22], [23].

Correlators feature a rapid switching time of around 10 ms, exhibit an isolation level, surpassing -80 dB between channels, and maintain a repeatability variation of approximately 0.01 dB under consistent conditions. These features showcase a distinct advantage by requiring

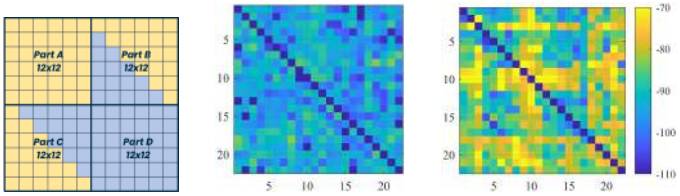

(a) (b) (c)

Fig. 2. (a) Filling Procedure of the 24×24 scattering matrix using two correlators and the four-port VNA; (b) differential scattering matrix between two identical situations and (c) between case with and without stroke. The colorbar is in [dB].

a briefer stabilization time after each cycle compared to electromechanical switches, thus reducing acquisition time. However, the overall measuring duration remains governed by the VNA setting.

As shown in Fig. 1, the implemented architecture connects the four-port VNA with two 4×16 correlators, dubbed C_L and C_R in the scheme, where L and R refer to left and right, respectively. So, it's notable that it does not use two of the input ports of each correlator, and only the 1:12 output channels are employed. This configuration adapts the available off-the-shelf product to our specific problem but leaves room for the potentially simplified 4×16 system or an extended 4×32 one. Then, to compile a full 24×24 scattering matrix, the acquisition process gathers independently the sections A and D in Fig. 2(a), $S_{1:11}$ and $S_{12:24}$, using C_L and C_R, respectively. Subsequently, the two additional B and C sections are filled out using C_L and C_R simultaneously. Though, the imaging uses 22×22 input matrices, two additional channels are proposed for environmental calibration [24].

C. *Radiation Unit: Antenna-Matching Cell*

We develop a third optimized and simplified antenna version starting from the ones presented in [25] and [17]. This consists of an Antenna-Matching Cell (Ant-MM) as shown in Fig. 3, that joins a printed monopole antenna on a slab of 1.55 mm thickness FR4, ϵ_r = 4.4, and σ = 0.012 S/m with a dielectrically custom-made matching medium composed of 30% graphite powder and 70% urethane rubber, named G30, with ϵ_r = 19 and σ = 0.15 S/m at 1 GHz. Consistent with [26], the antenna is designed to operate about 1 GHz,

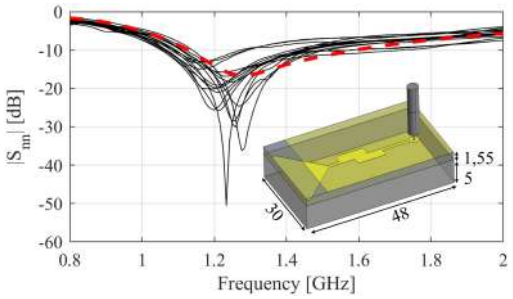

Fig. 3. Reflection coefficients amplitude; each black line corresponds to the n-th antenna of the MWI system, with n = 1:22; the red dotted one is the result of a simulation. The antenna dimensions are in (mm).

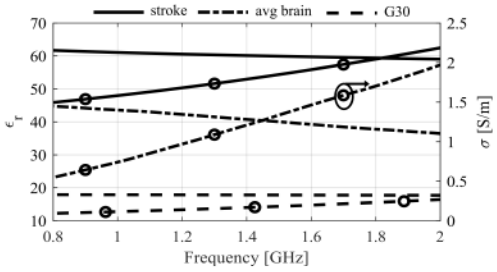

Fig. 4. Permittivity and conductivity of hemorrhagic stroke, average brain and G30.

achieving a good trade-off between penetration inside the head tissues and spatial imaging resolution. Compared to the second version [17], this eases the manufacturing process, reducing the variability and, therefore, the modeling error while keeping its performance, both essential aspects for the imaging. Moreover, compared to more complex designs such as [27], [28], the simplified design allows easier modeling by the inversion algorithm, and manufacturing process. Also, it could be a candidate to be enhanced using metasurfaces [29].

The reflection coefficients of the antennas are depicted in Fig. 3, where each continuous black line represents an antenna placed around a single-cavity head phantom filled with an alcohol-based liquid mimicking the average brain as shown in Fig. 1, and the reference dotted red line came from simulation placing the antenna in front of a homogeneous block with the average brain properties. Hence, the variability is due to the antenna positioning and the inevitable manufacturing tolerance of each home-made antenna.

III. Experimental Validation

A. Experimental Setup

We follow a similar testing scheme in [17] to validate the system, driven by our primary goal of testing the new solid-state switching matrices and radiating elements. Hence, we opt for a simplified hemorrhagic scenario using a 3-D-printed phantom inspired by the one in [30] and an evolving stroke model with a balloon filled with alcohol-based liquids [17]. In this case, we present a two-step experiment representing the evolution of a stroke scenario from healthy to a 20 ml one and then to 40 ml. The permittivity and conductivity of the mimicking liquids are depicted in Fig. 4, which are characterized using Keysight's "N1500a materials measurement suite" software [31]. Also, we used the hybrid method in [32] to characterize the solid mixture to match the antenna.

B. Results

Fig. 5(a-b) shows the imaging reconstruction results, representing the 3-D normalized dielectric contrast maps. In each, the yellow area indicates the change in the affected area and is denoted by the values above -3 dB. These demonstrate how the system can track and localize the evolution, as highlighted by the counter lines in the Fig. 5(b-d), which indicates the estimated position and shape of the target while receiving as input differential scattering matrix like the ones in Fig. 2(b-c). The imaging capabilities and performance remains equivalent to the ones in [17], highlighting the advantage of more stable switching. The improvement in switching time is at least 3x in such a basic configuration.

IV. Conclusions and Perspectives

This research introduces a low complexity and portable pMWI system tailored for diagnosis and real-time follow-up of the stroke, emphasizing the integration of state-of-the-art solid-state correlators. The adoption of these switches, in contrast to electromechanical counterparts, results in a more stable and fast switching speeds and enhanced device compactness, while maintaining imaging capabilities. Experimental validation underscores the system's accuracy in pinpointing a simulated stroke, accentuating its potential for practical applications in stroke monitoring in real time. For future endeavors, the results demonstrated in the experimental validation on a homogeneous phantom are planned to be extended to complex realistic scenarios. Moreover, additional classification capabilities and enhanced resolution imaging exploiting machine learning algorithms will be explored [33], [34], as well as calibration schemes such as [35], [36] that make the imaging process more robust.

Acknowledgment

This work was supported in part by the project PON Research and Innovation "Microwave Imaging and Detection powered by Artificial Intelligence for Medical and Industrial Applications (DM 1062/21)", funded by MUR. It was carried out partially in part within the Agritech National Research Center, funded by the European Union Next-Generation EU (Piano Nazionale di Ripresa e Resilienza (PNRR) – MISSIONE 4 COMPONENTE 2, INVESTIMENTO 1.4 – D.D. 1032 17/06/2022, CN00000022); in part within

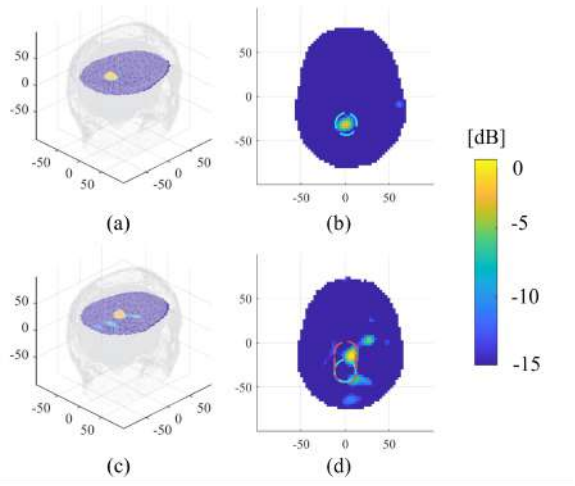

Fig. 5. Monitoring of HS progression. (a) 3-D normalized dielectric contrast sliced in the middle of the stroke region and (b) transverse view of case 0 (healthy) - 20 ml. (c) 3-D normalized dielectric contrast sliced in the middle of the stroke region and (d) transverse view of case 20 ml - 40 ml

the research project “MedWaveImage - Microwave imaging technology transfer to innovate the medical sector”, funded by Interreg Central Europe (CE0200670) and in part within the research project “3BAtwin - Bone, Brain, Breast and Axillary Medical Microwave Imaging Twinning” funded by Horizon Europe Framework Programme (101159623).

We thank Prof. J.Ch. Bolomey (University Paris-Saclay) for fruitful discussions and eV-Technologies for providing us with the correlators.

REFERENCES

[1] C. W. Tsao, A. W. Aday, Z. I. Almarzooq, *et al.*, “Heart disease and stroke statistics—2022 update: A report from the american heart association,” *Circulation*, vol. 145, no. 8, e153–e639, 2022.

[2] K. B. Walsh, “Non-invasive sensor technology for prehospital stroke diagnosis: Current status and future directions,” *International journal of stroke*, vol. 14, no. 6, pp. 592–602, 2019.

[3] S. Mathur, S. Walter, S. A. Helwig, and M. Lesmeister, “Improving prehospital stroke services in rural and underserved settings with mobile stroke units,” *Frontiers in neurology*, vol. 10, p. 439 167, 2019.

[4] S. Shahrestani, D. Wishart, S. M. J. Han, *et al.*, “A systematic review of next-generation point-of-care stroke diagnostic technologies,” en, *Neurosurg Focus*, vol. 51, no. 1, E11, 2021. DOI: 10.3171/2021.4.FOCUS21122.

[5] S. Chennareddy *et al.*, “Portable stroke detection devices: A systematic scoping review of prehospital applications,” *BMC Emergency Medicine*, vol. 22, no. 1, p. 111, 2022, ISSN: 1471-227X. DOI: 10.1186/s12873-022-00663-z. [Online]. Available: https://doi.org/10.1186/s12873-022-00663-z.

[6] S. Patil, R. Rossi, D. Jabrah, and K. Doyle, “Detection, diagnosis and treatment of acute ischemic stroke: Current and future perspectives,” *Frontiers in Medical Technology*, vol. 4, 2022, ISSN: 2673-3129. DOI: 10.3389/fmedt.2022.748949. [Online]. Available: https://www.frontiersin.org/articles/10.3389/fmedt.2022.748949.

[7] M. H. Mazurek *et al.*, “Portable, bedside, low-field magnetic resonance imaging for evaluation of intracerebral hemorrhage,” *Nature Communications*, vol. 12, no. 1, p. 5119, 2021, ISSN: 2041-1723. DOI: 10.1038/s41467-021-25441-6. [Online]. Available: https://doi.org/10.1038/s41467-021-25441-6.

[8] T.-O. Liang, Y. H. Koh, T. Qiu, E. Li, W. Yu, and S. Y. Huang, “High-performance permanent magnet array design by a fast genetic algorithm (ga)-based optimization for low-field portable mri,” *Journal of Magnetic Resonance*, vol. 345, p. 107 309, 2022, ISSN: 1090-7807. DOI: https://doi.org/10.1016/j.jmr.2022.107309. [Online]. Available: https://www.sciencedirect.com/science/article/pii/S1090780722001677.

[9] *Micro-x*, Available at https://micro-x.com/products/ct-brain-scanner/.

[10] A. Fhager, S. Candefjord, M. Elam, and M. Persson, “Microwave diagnostics ahead: Saving time and the lives of trauma and stroke patients,” *IEEE Microwave Magazine*, vol. 19, no. 3, pp. 78–90, 2018. DOI: 10.1109/MMM.2018.2801646.

[11] L. Guo, A. S. Alqadami, and A. Abbosh, “Stroke diagnosis using microwave techniques: Review of systems and algorithms,” *IEEE Journal of Electromagnetics, RF and Microwaves in Medicine and Biology*, vol. 7, no. 2, pp. 122–135, 2022.

[12] D. Cook *et al.*, “Case report: Preliminary images from an electromagnetic portable brain scanner for diagnosis and monitoring of acute stroke,” en, *Front Neurol*, vol. 12, p. 765 412, 2021.

[13] A. Abbosh *et al.*, “Clinical electromagnetic brain scanner,” *Scientific Reports*, vol. 14, no. 1, p. 5760, 2024, ISSN: 2045-2322. DOI: 10.1038/s41598-024-55360-7. [Online]. Available: https://doi.org/10.1038/s41598-024-55360-7.

[14] A. Fedeli, V. Schenone, A. Randazzo, M. Pastorino, T. Henriksson, and S. Semenov, “Nonlinear s-parameters inversion for stroke imaging,” *IEEE Transactions on Microwave Theory and Techniques*, vol. 69, no. 3, pp. 1760–1771, 2021. DOI: 10.1109/TMTT.2020.3040483.

[15] B. Norrving, “Classification of stroke subtypes,” *Stroke. Practical guide for clinicians. Karger: Basel*, p. 50, 2009.

[16] J. A. Tobon Vasquez, R. Scapaticci, G. Turvani, *et al.*, “A prototype microwave system for 3d brain stroke imaging,” *Sensors*, vol. 20, no. 9, p. 2607, 2020.

[17] D. O. Rodriguez-Duarte, C. Origlia, J. A. T. Vasquez, R. Scapaticci, L. Crocco, and F. Vipiana, “Experimental assessment of real-time brain stroke monitoring via a microwave imaging scanner,” *IEEE Open Journal of Antennas and Propagation*, vol. 3, pp. 824–835, 2022.

[18] *Dual evt1016*, Available at https://ev-technologies.com/portfolio-items/dual-evt1016/.

[19] J. A. Tobon Vasquez, R. Scapaticci, G. Turvani, *et al.*, “Design and experimental assessment of a 2d microwave imaging system for brain stroke monitoring,” *International Journal of Antennas and Propagation*, vol. 2019, pp. 1–12, 2019.

[20] D. O. Rodriguez-Duarte, J. A. T. Vasquez, R. Scapaticci, L. Crocco, and F. Vipiana, “Assessing a microwave imaging system for brain stroke monitoring via high fidelity numerical modelling,” *IEEE Journal of Electromagnetics, RF and Microwaves in Medicine and Biology*, vol. 5, no. 3, pp. 238–245, 2021. DOI: 10.1109/JERM.2020.3049071.

[21] *Keysight*, Available at https://www.keysight.com/us/en/product/\\P9375A/streamline-usb-vector-network-analyzer-26-5-ghz.html.

[22] N. Valizade Shahmirzadi, N. K. Nikolova, and C.-H. Chen, “Interconnect for dense electronically scanned antenna array using high-speed vertical connector,” *Sensors*, vol. 23, no. 20, 2023, ISSN: 1424-8220. DOI: 10.3390/s23208596. [Online]. Available: https://www.mdpi.com/1424-8220/23/20/8596.

[23] O. Zaatar, A. Zakaria, and N. Qaddoumi, “A novel switch for microwave imaging systems,” *IEEE Access*, vol. 12, pp. 26 978–26 990, 2024. DOI: 10.1109/ACCESS.2024.3367355.

[24] D. O. Rodriguez-Duarte, J. A. Tobon Vasquez, R. Scapaticci, *et al.*, “Experimental validation of a microwave system for brain stroke 3-d imaging,” *Diagnostics*, vol. 11, no. 7, p. 1232, 2021.

[25] D. O. Rodriguez-Duarte, J. A. T. Vasquez, R. Scapaticci, L. Crocco, and F. Vipiana, “Brick-shaped antenna module for microwave brain imaging systems,” *IEEE Antennas and Wireless Propagation Letters*, vol. 19, no. 12, pp. 2057–2061, 2020.

[26] R. Scapaticci, J. Tobon, G. Bellizzi, F. Vipiana, and L. Crocco, “Design and numerical characterization of a low-complexity microwave device for brain stroke monitoring,” *IEEE Transactions on Antennas and Propagation*, vol. 66, no. 12, pp. 7328–7338, 2018.

[27] M. Salimitorkamani, M. Mehranpour, and H. Odabasi, “A miniaturized wideband sinuous antenna for microwave brain imaging systems,” *IEEE Transactions on Antennas and Propagation*, vol. 72, no. 3, pp. 2228–2240, 2024. DOI: 10.1109/TAP.2024.3355232.

[28] H. Chen and K.-M. Luk, “Detection capability enhanced biosensor antenna for portable electromagnetic stroke diagnostic systems,” *IEEE Transactions on Biomedical Circuits and Systems*, vol. 18, no. 1, pp. 145–159, 2024. DOI: 10.1109/TBCAS.2023.3313732.

[29] D. Brizi, M. Conte, and A. Monorchio, “A performance-enhanced antenna for microwave biomedical applications by using metasurfaces,” *IEEE Transactions on Antennas and Propagation*, vol. 71, no. 4, pp. 3314–3323, 2023. DOI: 10.1109/TAP.2023.3242414.

[30] N. Joachimowicz, B. Duchêne, C. Conessa, and O. Meyer, “Anthropomorphic breast and head phantoms for microwave imaging,” *Diagnostics*, vol. 8, no. 4, p. 85, 2018.

[31] *Keysight*, Available at https://www.keysight.com/us/en/product/\\P9375A/streamline-usb-vector-network-analyzer-26-5-ghz.html.

[32] M. Gugliermino, D. O. Rodriguez-Duarte, J. A. T. Vasquez, M. Lumia, G. Virone, and F. Vipiana, “Hybrid simulation-measurement method for broadband dielectric characterization of synthetic human head tissues,” in *2023 IEEE Conference on Antenna Measurements and Applications (CAMA)*, IEEE, 2023, pp. 17–21.

[33] Á. Yago Ruiz, M. Cavagnaro, and L. Crocco, “An effective framework for deep-learning-enhanced quantitative microwave imaging and its potential for medical applications,” *Sensors*, vol. 23, no. 2, p. 643, 2023.

[34] V. Mariano, J. A. Tobon Vasquez, M. R. Casu, and F. Vipiana, “Brain stroke classification via machine learning algorithms trained with a linearized scattering operator,” *Diagnostics*, vol. 13, no. 1, p. 23, 2022.

[35] S. Cathers, J. LoVetri, I. Jeffrey, and C. Gilmore, “Electromagnetic imaging system calibration with 2-port error models,” *IEEE Open Journal of Antennas and Propagation*, vol. 4, pp. 1142–1153, 2023. DOI: 10.1109/OJAP.2023.3329356.

[36] B. Martin, K. Edwards, I. Jeffrey, and C. Gilmore, “Experimental microwave imaging system calibration via cycle-gan,” *IEEE Transactions on Antennas and Propagation*, vol. 71, no. 9, pp. 7491–7503, 2023. DOI: 10.1109/TAP.2023.3296915.